Investigation of the moisture damage and the erosion depth on asphalt

Zou, Yingxue; Xu, Haiqin; Xu, Shi; Chen, Anqi; Wu, Shaopeng; Amirkhanian, Serji; Wan, Pei; Gao, Xiang

DOI
10.1016/j.conbuildmat.2023.130503

Publication date
2023

Document Version
Final published version

Published in
Construction and Building Materials

Construction and Building Materials 369 (2023) 130503

Contents lists available at ScienceDirect

Construction and Building Materials

journal homepage: www.elsevier.com/locate/conbuildmat

Investigation of the moisture damage and the erosion depth on asphalt

Yingxue Zou [a], Haiqin Xu [a], Shi Xu [b,c,*], Anqi Chen [a,*], Shaopeng Wu [a], Serji Amirkhanian [d], Pei Wan [a], Xiang Gao [a]

[a] State Key Laboratory of Silicate Materials for Architectures, Wuhan University of Technology, Luoshi Road 122, Wuhan 430070, China
[b] School of Civil Engineering and Architecture, Wuhan University of Technology, Luoshi Road 122, Wuhan 430070, China
[c] Faculty of Civil Engineering and Geosciences, Delft University of Technology, Stevinweg 1, 2628 CN Delft, the Netherlands
[d] Department of Civil Construction and Environmental Engineering, University of Alabama, Tuscaloosa, AL 35487, USA

ARTICLE INFO

Keywords:
Asphalt
Moisture damage
Rheological property
Adhesion property
Erosion depth
Diffusion coefficient

ABSTRACT

Moisture erosion is one of the key factors leading to asphalt pavement damage, and the erosion depth indicates the moisture damage level but it is usually neglected. In order to study the moisture erosion and the erosion depth, this study characterized the chemical structure, rheological property and adhesion property of asphalt at different depths after immersion for different periods. To further explore the diffusion mechanism of eroded asphalt, a Log-log numerical model was established based on the Fick's second law to calculate the diffusion coefficient throughout the depth. The results indicate that it takes just four hours for water to penetrate a 25 μm asphalt film. The relation between erosion depth and immersion period presents three stages, and the process can be fitted with a polynomial model. At the macroscopic level, there is a lag between the changes in adhesion property with chemical structure and rheological property. Additionally, the periodicity of moisture erosion process was verified by the calculation of diffusion factor. In summary, the diffusion mechanism of eroded asphalt by moisture can provide a theoretical basis for the development of laboratory moisture erosion test specification, thus avoiding the waste of raw materials.

1. Introduction

Asphalt pavement is a kind of seamless continuous pavement with the excellent pavement performance and driving comfort, which are widely utilization in the world [1]. Nevertheless, the degradation of pavement performance has always been the primary problem in the field, and the moisture damage is one of the most important inducements [2]. During the service period, asphalt pavement is inevitably eroded by common fluids such as rainwater, ground water, etc. The fluids penetrate and erode asphalt concrete through its voids, therefore adversely affecting the structure and performance of asphalt mixture [3]. More attentions were paid on the destructive effects of dynamic hydraulic pressure and freeze–thaw cycles [4]. However, the failure of cohesion and adhesion is the internal root causes of moisture damage on asphalt mixture [5]. The asphalt film may be dissolved and peel off from the aggregate surface because of the existence of moisture. Therefore, the hydrostatic erosion test is more suitable to study the erosion effect and related mechanism of moisture as a single factor on asphalt. Besides, the other studies of hydrostatic erosion test have focused on the change of composition, structure, cohesion and adhesion of asphalt during moisture erosion. The results show that water diffusion can increase the enriched polar components, causing the degradation of rheological property, cohesion and adhesion property [6]. The oxidation, dissolution and migration of asphalt is considered to affect the physicochemical properties of asphalt during immersion [7].

In an asphalt mixture, asphalt is acting as the binding material in the form of a thin film and bonds the aggregate surfaces together [8]. Asphalt binder is available in the form of asphalt film, which bonds the aggregate interface to make asphalt concrete with outstanding road performance [9]. In principle, the asphalt film thickness is approximately 6–15 μm which is determined by the asphalt content and aggregate surface area [10]. However, this number can increase to 26 μm due to the uneven binder distribution in practice [11,12]. The optimum asphalt content and aggregate surface area collectively

* Corresponding authors at: School of Civil Engineering and Architecture, Wuhan University of Technology, Luoshi Road 122, Wuhan 430070, China (S. Xu). State Key Laboratory of Silicate Materials for Architectures, Wuhan University of Technology, Luoshi Road 122, Wuhan 430070, China (A. Chen).
E-mail addresses: zouyingxue@whut.edu.cn (Y. Zou), xuhaiqin@whut.edu.cn (H. Xu), xushi@whut.edu.cn (S. Xu), anqi.chen@whut.edu.cn (A. Chen), wusp@whut.edu.cn (S. Wu), samirkhanian@eng.ua.edu (S. Amirkhanian), wanpei@whut.edu.cn (P. Wan), 303725@whut.edu.cn (X. Gao).

https://doi.org/10.1016/j.conbuildmat.2023.130503
Received 4 July 2022; Received in revised form 29 December 2022; Accepted 20 January 2023
Available online 2 February 2023

determine the effective thickness of asphalt film [13]. During the mixing of asphalt and aggregate, a rearrangement of chemical components of the asphalt is produced on the mineral surface due to the chemisorption that occurs as a result of the interaction between asphalt and mineral, thus creating a structural film on the mineral surface [14]. The structural film is known as structural asphalt, and the asphalt outside the film is known as free asphalt. The cohesion of structural asphalt is greater than that of free asphalt [15]. Asphalt has different properties and functions at different distances from the aggregate contact interface, and the changes in properties can cause different effects [16]. Therefore, exploring the erosion depth of asphalt by aqueous solution is the key to understand the changes in water stability of asphalt concrete.

Researchers have paid attention to the impact of asphalt film thickness on water stability. Dos Santos et al. [17] employed the atomic force microscope to study bitumen films within 300 μm thickness after being immersed in aqueous solution. By observing the microstructure changes, they found moisture could cause the dissolution and migration of asphalt, making the asphalt thinner and the properties change. Burak Sengoz et al. [10] investigated the relation between the asphalt film thicknesses and water stability of hot mix asphalt, and the results manifested asphalt mixture with a thicker asphalt film showed better water stability. Yan et al [18] designed the binder bond strength test to investigate the effect of asphalt film thickness on bond strength between asphalt and aggregate under wet curing conditions, and they inferred the thicker thickness of asphalt film had a positive effect on bonding properties. Lin [19] compared the performance of asphalt mixture with different film thickness and found that the asphalt film thickness and the water stability of mixture had nonlinear relation, and the water stability decreased sharply when the film thickness was less than 13 μm. Based on the above results, the asphalt film thickness plays the important role in the pavement performance, and the moisture can weaken asphalt properties. The relevant researchers used asphalt film with 0.1–2 m thick for hydrostatic erosion tests, however, no justification or specification for the selection was given [20]. Furthermore, the erosion depth by moisture on asphalt binder and the properties changes of asphalt film at different depths lack investigation. Therefore, the study of erosion depth on asphalt is an important guide for the scientific selection of asphalt thickness in future simulated hydrostatic erosion tests.

In this study, the moisture damage and the erosion depth on asphalt was investigated, and the methodological framework was illustrated in Fig. 1. First, 90 A and SBS MA were immersed in the distilled water at 60 °C for different periods. Then, the asphalt samples were obtained by being stripped away layer by layer. The chemical structure, rheological property and adhesion property of asphalt were characterized by Fourier transform infrared spectroscopy (FTIR) analysis, dynamic shear rheometer (DSR) analysis and contact angle (CA). By comparing the properties of different layers, the relation between erosion depth and immersion period was discussed. Subsequently, the correlation between carbonyl index ($I_{C=O}$), fatigue factor (*FF*) and energy ratio (*ER*) were discussed by Pearson correlation coefficient. Based on the Fick's second law, a simple Loglog model was established to simulate the diffusion of eroded asphalt during immersion and calculate the diffusion coefficient of different layers. Finally, the diffusion mechanism of eroded asphalt by moisture was explored based on the diffusion model.

2. Materials and experiments

2.1. Materials

Base 90 asphalt (90 A) with 80/100 penetration grade and performance grade 70–22 and styrene–butadiene–styrene Modified Asphalt (SBS MA) were used in this research. The two kinds of asphalt were

Table 1
Physical properties of 90 A and SBS MA.

Physical properties	Units	90 A	SBS MA	Standards
Penetration (25 °C, 100 g, 5 s)	0.1 mm	86.7	63.5	ASTM D-5 [22]
Softening point	°C	46.8	75.3	ASTM D-36 [23]
Ductility (10 °C/5 °C)	cm	89	56	ASTM D-113 [24]
Solubility (trichloroethylene)	%	99.8	99.7	ASTM D-2042 [25]

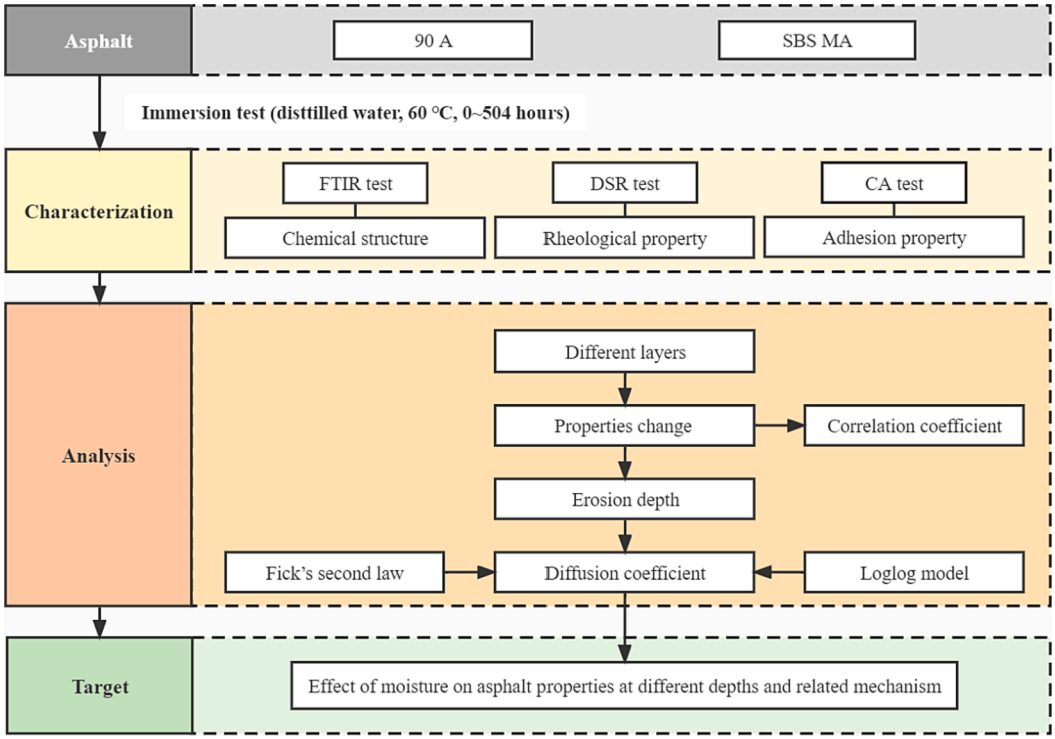

Fig. 1. Methodological framework of this study.

obtained from Inner Mongolia Xindalu Asphalt CO., ltd (Inner Mongolia, China), and the basic physical properties were illustrated in Table 1. Limestone provided by Wuhan Jiuhua Co., ltd (Wuhan, China) was selected as the aggregates, due to its stable properties and wide distribution [21].

2.2. Immersion test

The immersion test simulated the erosion of moist environment on asphalt pavement. Because the influence of water on asphalt mainly occurs during the service period, using asphalt binders after TFOT instead of unaged asphalt binders as the samples of water erosion can more truly simulate the influence of water on asphalt in the pavement. First, 8 g 90 A after thin film oven test (TFOT) was poured into the glass dish with a diameter of 90 mm, then placed in a vacuum drying box at 150 °C for 0.5 h next. After cooling, the 1.25 mm thick asphalt film was prepared. Second, the distilled water was poured into the glass dish soaking the asphalt film completely. The experimental temperature was set at 60 °C because it was close to the road temperature in summer. The asphalt was undertaken for immersion of 4, 6, 12, 48, 96, 144, 288, 336, 432 and 504 h, and the aqueous solution was changed every other day to ensure the moist environment. Finally, the asphalt films were dried in the oven at 100 °C for 15 mins and cooled to room temperature for one day to dry the water on the surface of asphalt film. The SBS MA samples were obtained under the same condition. In the meantime, control samples were prepared at the same periods without water immersion. Four parallel aging tests were conducted simultaneously to collect enough asphalt samples for testing, because FTIR test, DSR test and CA test typically requires around 0.1 g, 0.4 g and 0.2 g asphalt respectively.

2.3. Peeling test

Peeling test was designed to explore the influence of moisture on asphalt at different depths, as shown in Fig. 2. The experiment was divided into the following five steps.

i. 5 ml trichloroethylene as organic solvent was poured into the glass dish to dissolve the surface of asphalt film;
ii. The solution with dissolved asphalt was poured out in a glass dish with a diameter of 90 mm and placed in a fume cupboard for 72 h to allow trichloroethylene to evaporate completely, and the layer 1 of asphalt film was obtained [26];
iii. The physicochemical properties of layer 1 were compared with that of control by FTIR analysis, DSR analysis and CA analysis;
iv. The peeling experiment would be repeated from step i on the residual asphalt film when the physicochemical properties of the peeling layer was inconsistent with that of control;
v. The peeling experiment stop until the physicochemical properties were consistent with that of control, and the peeling depth was determined as the erosion depth.

The film thickness of peeled asphalt was calculated by Eq. (1).

$$T = \frac{m}{\pi r^2 \rho} \tag{1}$$

where T, m and ρ represent the thickness, mass and density of asphalt film, respectively; r represents the radius of the glass dish.

According to the preliminary test, it took 11 s for the first film with around 25 μm on the sample surface, while only 6 s for the internal asphalt with around 25 μm thickness, and 13 s for the 50 μm internal layer. The peeling test was carried out with the same operation procedure for each sample, so as to ensure the same film thickness as far as possible, and the calculated film thickness was taken as the final film thickness. According to the result of FTIR, DSR and CA tests of samples treated with trichloroethylene and the untreated based asphalt, there was no characteristic peak of trichloroethylene in the FTIR spectrogram, and the data gap was within the standard range, indicating that the trichloroethylene in the asphalt film had been volatilized completely after 3 days.

The asphalt collected from four parallel samples was mixed at 120 °C to achieve uniformity before tests. The asphalt immersed for different periods were peeled layer by layer to characterize the physicochemical properties, including chemical structure, rheological properties and CA. When used as a semi-quantitative analytical tool, the permissible error in FTIR is 3 % [8]. According to DSR test specification, the coefficient of variation (CV) of the fatigue factor (FF) as acceptable single-operator precision cannot exceed 4.9 % [27]. The CV of all CAs in parallel tests was lower than 4 % [28]. When the error value of the last peeled layer is within this range from the control sample, the layer is considered to own the same performance as the control sample. Additionally, it was found that the peel method had no significant effect on the test results by comparing the results of the unsoaked asphalt before and after the peel test. The thickness of different peeled asphalt layers was shown in Tables 2 and 3 respectively. The film thickness of each layer was planned to be around 25 μm, which contains the thickness of the asphalt film on the real pavement to expediently observe the performance change of asphalt under the real film thickness. Subsequently, different asphalt film thicknesses were obtained by adjusting the trichloroethylene dissolution time.

2.4. FTIR test

To investigate the change of chemical structure, FTIR (Nicolet 6700, Thermo Fisher Scientifific, Waltham, MA, USA) with OMNIC 6.2 software was used to identify the specific functional groups. First, 5 wt%

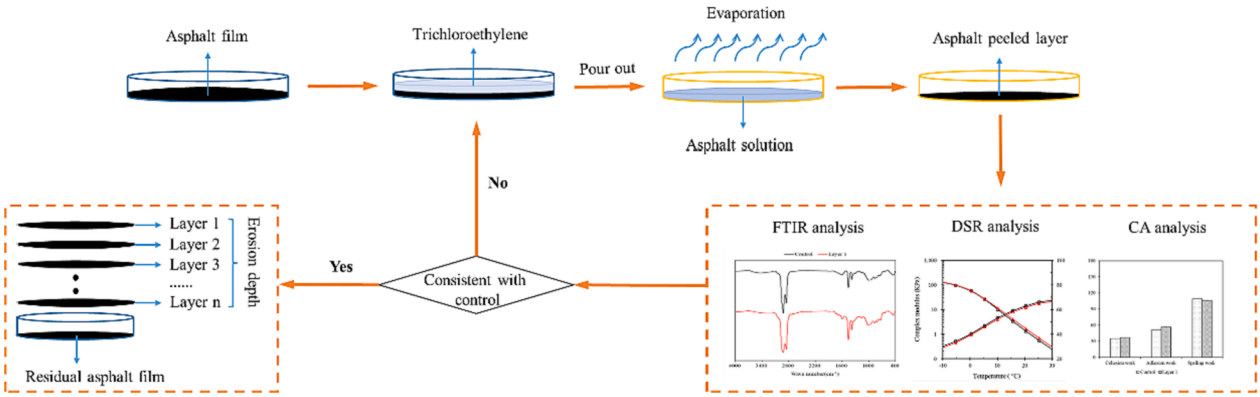

Fig. 2. Flow chart of asphalt peeling test.

Table 2
Film thickness of 90 A after peeling (μm).

Layer	Immersion period by distilled water (hour)									
	4	6	12	48	96	144	288	336	432	504
1	27	23	31	22	31	25	26	24	21	29
2	25	26	29	24	27	21	30	27	30	32
3	NA	54	48	56	55	57	64	57	52	60
4	NA	NA	53	59	54	65	59	59	54	59
5	NA	NA	NA	62	47	61	62	61	69	53
6	NA	NA	NA	NA	49	52	53	49	51	48
7	NA	NA	NA	NA	NA	49	58	54	50	58
8	NA	NA	NA	NA	NA	NA	45	54	50	52
9	NA	NA	NA	NA	NA	NA	NA	51	55	45
10	NA	NA	NA	NA	NA	NA	NA	NA	76	83
11	NA	NA	NA	NA	NA	NA	NA	NA	NA	82

Note: NA represents not available.

Table 3
Film thickness of SBS MA after peeling (μm).

Layer	Immersion period by distilled water (hour)									
	4	6	12	48	96	144	288	336	432	504
1	23	18	16	21	24	22	17	22	19	22
2	27	29	23	26	33	30	32	28	26	30
3	NA	33	31	37	41	43	32	37	34	35
4	NA	NA	55	46	54	60	65	69	67	63
5	NA	NA	NA	54	53	48	41	47	45	43
6	NA	NA	NA	NA	42	50	47	49	54	43
7	NA	NA	NA	NA	NA	45	59	56	54	57
8	NA	NA	NA	NA	NA	NA	28	27	23	23
9	NA	NA	NA	NA	NA	NA	NA	33	31	37
10	NA	NA	NA	NA	NA	NA	NA	NA	27	21
11	NA	NA	NA	NA	NA	NA	NA	NA	NA	27

asphalt-CS_2 solution was prepared, then three drops of the solution were dropped on the KBr chip. Finally, FTIR test was performed after CS_2 evaporated completely. The range of scan wave number was from 4000 cm^{-1} to 400 cm^{-1} and the scan time was 64 times. Although water can block oxygen from the air to some extent, asphalt can react with oxygen molecules from the water leading to asphalt oxidation during immersion [29]. And the dissolution and migration of asphalt also occur due to the existence of water [30]. That is considered to affect the physicochemical properties of asphalt. The oxidation products of asphalt oxidation and the majority of substances dissolved and migrated from asphalt are generally contains carbonyl and sulfoxide groups [7]. Because sulfoxide is a very unstable bond and can undergo reversible reactions with temperature and other conditions, while carbonyl is very stable. Therefore, carbonyl was selected to be the index. The $I_{C=O}$ was chosen to characterize the degree of asphalt oxidation calculated with Eq. (2) [31].

$$I_{C=O} = \frac{S_{1700cm^{-1}}}{S_{1462+1377cm^{-1}}} \quad (2)$$

where S^{-1}_{1700cm} represents the areas of the 1700 cm^{-1} centered carbonyl group absorption band; $S^{-1}_{1462+1377cm}$ represents the sum of areas of the 1462 cm^{-1} centered methylene group absorption band and 1377 cm^{-1} centered methyl group absorption band.

2.5. DSR test

The temperature sweep using DSR (Smartpave 102, Anton Paar Co. ltd, Germany) was selected to analyze low temperatures rheological property of asphalt after immersion. The deformation was measured under fixed frequency sinusoidal loading, which was characterized by complex shear modulus (G*) and phase angle (δ) [32,33]. The asphalt samples with a diameter of 8 mm and a thickness of 2 mm were prepared for the test. Table 4 showed the test parameters of temperature sweep.

Table 4
Test parameters of temperature sweep.

Projects	Frequency	Strain	Temperature	Heating rate
Units	rad/s	%	°C	°C/min
Parameters	10	0.5	−10–30	2

2.6. CA test

The surface free energy (SFE) of asphalt is related to the cohesion inside the binder and the adhesion between asphalt binder from different depths with aggregate. The sessile drop method is the most commonly used method to measure the CA of liquid on solid, which is usually used to calculate the SFE of asphalt. The CA measuring instrument (SL150, KINO Industry Co. ltd, USA) with Image processing software was used to magnify the contour of liquid drop and solid and measure the CA. The CA of limestone was measured by the probe liquids, including distilled water, formamide and glycol, while that of asphalt was measured using distilled water, formamide and glycerol. In order to guarantee the preciseness of the results, each group of 3 specimens was tested three times, the average test value was the final result. The number of samples should be increased to ensure that the CV of CA in parallel tests was lower than 4 % when the individual test results differ greatly [28].

The SFE could be calculated by the dispersion component and the polar component, which is the sum of them, as shown in Eq. (3) [34].

$$\gamma = \gamma^d + \gamma^p \quad (3)$$

where γ^d,γ^p represent dispersive component and polarity component of the SFE, respectively.

Owens and Wendt [35] came up with Eq (4) that accurately expressed the relation between the CA with the SFE. The polarity

component and dispersion component can be obtained by linear analysis of the test data according to the following equation.

$$\frac{\gamma_L(1+\cos\theta)}{2}\frac{1}{\sqrt{\gamma_L^d}}=\sqrt{\gamma_s^p}\sqrt{\frac{\gamma_L^p}{\gamma_L^d}}+\sqrt{\gamma_s^d} \tag{4}$$

where γ_S,γ_L represent SFEs of the solid and the liquid, respectively; γ_s^d,γ_s^p represent dispersive component and polarity component of the SFE for the solid; γ_L^d,γ_L^p represent dispersive component and polarity component of SFE for the liquid.

Table 5 showed the SFE parameters of the four probe liquids and limestone obtained by CA test [36].

The energy required for cracks to expand along the interface between the asphalt with aggregate is called adhesion work, which represents the difficulty of moisture penetrating the asphalt film into the asphalt-aggregate interface and can be defined as shown in Eq. (5) [37].

$$W_{am}=\gamma_a+\gamma_m-\gamma_{am}=2\sqrt{\gamma_a^d\gamma_m^d}+2\sqrt{\gamma_a^p\gamma_m^p} \tag{5}$$

where γ_a, γ_m and γ_{am} express SFEs of asphalt, mineral and the interface of asphalt and mineral, respectively. The γ_a^d and γ_a^p express the dispersive component and polarity component of asphalt, and γ_m^d and γ_m^p express the dispersive component and polarity component of mineral.

The adsorption effect of aggregate on water is greater than that on asphalt, and the asphalt is constantly peeled off from the surface of aggregate through the displacement of water, which eventually causes water damage of asphalt pavement. In this process, the bitumen-mineral aggregate system becomes bitumen-water and mineral aggregate-water two systems. And the work of process is defined as the spalling work as shown in Eq. (6).

$$\begin{aligned}W_{amw}&=W_{aw}+W_{mw}-W_{am}\\&=2\left(\sqrt{\gamma_a^d\gamma_w^d}+\sqrt{\gamma_a^p\gamma_w^p}+\sqrt{\gamma_m^d\gamma_w^d}+\sqrt{\gamma_m^p\gamma_w^p}-\sqrt{\gamma_a^d\gamma_m^d}-\sqrt{\gamma_a^p\gamma_m^p}\right)\end{aligned} \tag{6}$$

where W_{aw} and W_{mw} express the adhesion work between asphalt and mineral with water, respectively. The γ_w^d and γ_w^p express the dispersive component and polarity component of water.

The energy ratio (ER) is considered to evaluate the adhesion property of the asphalt binder as shown in Eq. (7).

$$ER=\left|\frac{W_{am}}{W_{amw}}\right| \tag{7}$$

The higher the *ER* value, the better the adhesion property of the asphalt-aggregate combination.

2.7. Correlation analysis

In order to explore the correlation between the three indicators, including $I_{C=O}$, *FF* and *ER*, during moisture erosion, statistical software SPSS 22.0 was used to conduct correlation analysis on the data. Bivariate correlation reflects the degree of correlation between two variables, which is usually explained by Pearson correlation coefficient. The calculation formula is shown in Eq. (8).

Table 5
SFE parameters of the probe liquids and aggregate (mJ/m^2).

	γ	γ_L^d	γ_L^p
Distilled water	72.8	21.8	51.0
Formamide	57.9	38.9	19.0
Glycol	48.3	29.3	19.0
Glycerol	63.4	33.4	30.0
Limestone	37.49	28.06	9.43

$$r=\frac{S_{ab}}{\sqrt{S_{aa}S_{bb}}} \tag{8}$$

where r is the correlation coefficient between variate a and b, S_{ab} is the covariance between variate a and b, S_{aa} is the variance of variate a, and S_{bb} is the variance of variate b.

2.8. Diffusion theories

(1) Fick's second law.

When the concentration gradient of components exists in the asphalt system, the concentration of any point in the asphalt will change with period, and the diffusion flux will also change with different positions. Macroscopically, the thermal movement components produce directionality, which will lead to the occurrence of diffusion in asphalt. Thus, the relation between erosion concentration with immersion period and depth can be obtained using the Fick' s second law which is suitable for unsteady diffusion, as shown in Eq. (9) [38].

$$\frac{\partial C}{\partial t}=D\frac{\partial^2 C}{\partial d^2} \tag{9}$$

where C and d express erosion concentration and depth of asphalt, respectively; D expresses diffusion coefficient; t expresses immersion period.

(2) Diffusion model setting up.

The reasonable diffusion model for moisture damage should be established to calculate the diffusion coefficient (D). Three necessary assumptions need to be proposed as follow. Firstly, moisture damage of asphalt is an unsteady diffusion form. Secondly, surface layer of asphalt suffers the most serious erosion, and the eroded asphalt diffuses internally with period. Finally, eroded asphalt and uneroded asphalt are treated as a pure substance without considering the composition of asphalt. Based on the assumptions above, a simple diffusion model of eroded asphalt under the action of moisture can be established as shown in Fig. 3.

Under the action of different concentration gradients, the eroded asphalt diffuses to the diffusion layer, and its diffusion depth increases with period. The erosion concentration in the outermost layer is affected by moisture erosion and internal diffusion, which can be regarded as constant. Lehtimäki proposed the Loglog model to predict the rheological properties of a mixture of two liquids [39]. Therefore, the erosion concentration of asphalt can be calculated by Loglog model as shown in Eq. (10).

$$\mathrm{loglog}\left(|FF|_{\mathrm{D}}\right)=a\mathrm{loglog}\left(|\mathrm{FF}|_{\mathrm{U}}\right)+b\mathrm{loglog}\left(|\mathrm{FF}|_{\mathrm{E}}\right) \tag{10}$$

where $|\mathrm{FF}|_{\mathrm{D}}$, $|\mathrm{FF}|_{\mathrm{U}}$ and $|\mathrm{FF}|_{\mathrm{E}}$ express *FF* of diffusion layer, uneroded asphalt and eroded asphalt, respectively. The $|\mathrm{FF}|_{\mathrm{D}}$ consists of only $|\mathrm{FF}|_{\mathrm{U}}$ and $|\mathrm{FF}|_{\mathrm{E}}$, and a is the proportion of $|\mathrm{FF}|_{\mathrm{U}}$ in the mixture $|\mathrm{FF}|_{\mathrm{D}}$, and b is the proportion of $|\mathrm{FF}|_{\mathrm{E}}$ in the mixture $|\mathrm{FF}|_{\mathrm{D}}$, thus $a+b=1$. Because the definition of C is also the proportion of $|\mathrm{FF}|_{\mathrm{E}}$ in the mixture $|\mathrm{FF}|_{\mathrm{D}}$, which is the same as the definition of b, C is equal to b.

Referring to Boltzmann change, definite integral concept and Eq. (11), the Eq. (9) can be transformed into Eq. (12) [40]. The boundary conditions are as follows: $C=C_1$ when x greater than 0, while $C=C_2$ when x less than 0.

$$\beta=\frac{x}{2\sqrt{Dt}} \tag{11}$$

$$C=\frac{C_1+C_2}{2}-\frac{C_2-C_1}{2}\frac{2}{\sqrt{\pi}}\int_0^{\beta}\exp\left(-\beta^2\right)d\beta+b \tag{12}$$

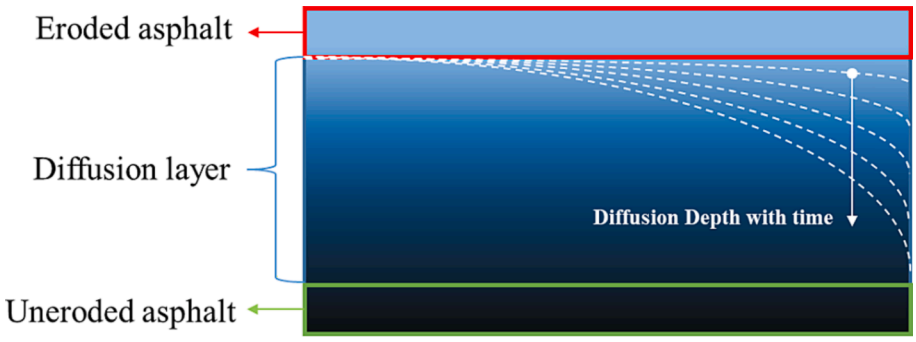

Fig. 3. Diffusion model of eroded asphalt under the action of moisture.

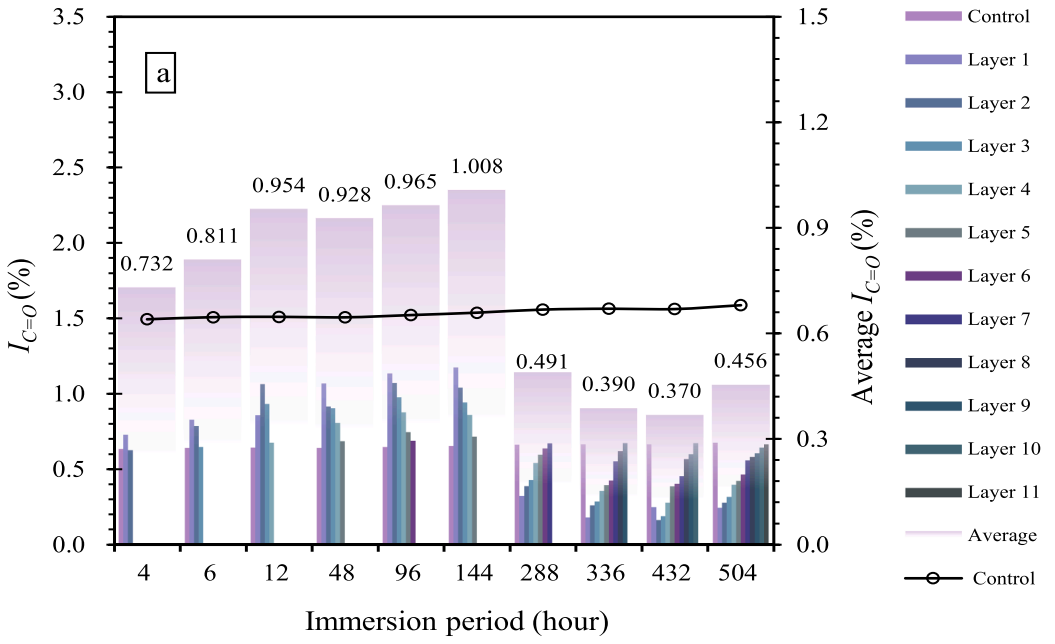

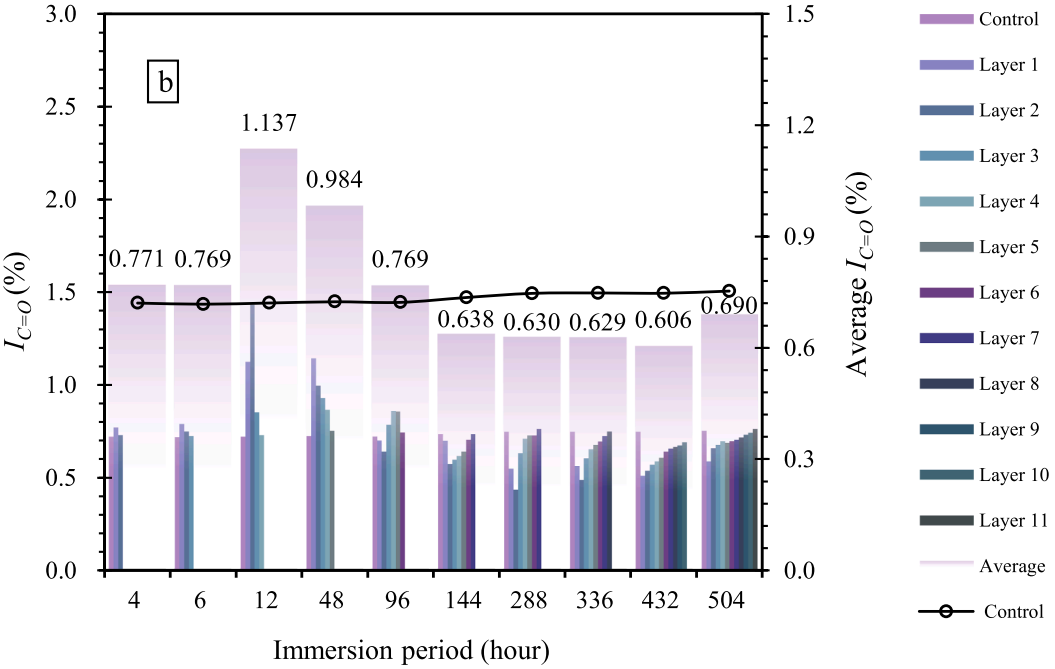

Fig. 4. $I_{C=O}$ of asphalt at different depths during immersion (a, 90 A; b, SBS MA).

In the semi-infinite object diffusion model, C_1 is equal to 0, C_2 is equal to 100 %. Because of the complexity of calculation, the Gaussian error equation is replaced by hyperbolic function as shown in Eq. (13), and MATLAB software was used in data processing.

$$C = 1 - tanh\left(\frac{993}{880}\beta + \frac{89}{880}\beta^3\right) \quad (13)$$

3. Results and discussions

3.1. Chemical structure

The changes in carbonyl groups is usually considered as an indicator of asphalt oxidation level [31]. The $I_{C=O}$ of different peeling layers in 90A and SBS MA were calculated according to FTIR spectrum to investigate changes in chemical structure of asphalt after immersion as shown in Fig. 4. The $I_{C=O}$ of all control samples at different periods was greater than 0, which was due to the fact that the control sample was prepared after TFOT aging. And the $I_{C=O}$ of control slightly increased with preparation time, because the curing temperature of 60 °C could cause the thermal oxidation of unsoaked asphalt during samples preparation. The $I_{C=O}$ of the layer 1 in 90A was greater than that of control during 4–144 h, indicating that moisture erosion caused oxidation of asphalt surface and produced more aging functional groups. Because asphalt can react with oxygen molecules from the water leading to oxidation of asphalt surface [29]. The $I_{C=O}$ of each layer inside asphalt increased gradually with the extension of erosion period, however the increasing rate decreased step by step from the surface to the inside, which might be caused by the diffusion of eroded asphalt. During 288 h-504 h of immersion, the $I_{C=O}$ of the layer 1 was lower than that of control, and the range of decline from the outside to the inside of a stepwise decline. That might be due to the predominant dissolution of polar functional groups containing carbonyl [7].

The $I_{C=O}$ of the layer 1 in SBS MA was greater than that of control during 4–48 h and less than that of control during 96–504 h. Compared with the control at 144 h, the $I_{C=O}$ of layers 1 and 2 decreased, while that of layers 3–5 increased, which might be the increase of $I_{C=O}$ caused by aging spread to layers 3–5, and the dissolution of polar components decreased the $I_{C=O}$ of layers 1 and 2. The change of $I_{C=O}$ in each layer of SBS MA at 4, 6, 48, 336, 432 and 504 h presented a step-like trend from surface to inside, which was the same as that of 90 A. In other periods, the maximum or minimum $I_{C=O}$ occurred in the layer 2. It is because the existence of the network structure of modifier in SBS MA can reduce the migration rate of polar components from the surface asphalt to the inner asphalt, changing the diffusion law of water erosion.

The average $I_{C=O}$ is the arithmetic average calculated by the carbonyl factors of all layers that have $I_{C=O}$ change during immersion. The variation pattern of the average $I_{C=O}$ was mostly dependent on that of the layer 1. The average $I_{C=O}$ of 90 A peaked at 144 h of immersion increasing by 50.39 %, and reached a trough after 432 h of immersion decreasing by 44.66 %. The average $I_{C=O}$ of SBS MA at 12 h increased to the maximum value by 56.53 %, and it decreased to the minimum value by 18.95 % at 432 h. It could be seen that oxidation reaction of SBS MA was dominant for a shorter period of time and entered the dissolution and migration dominant phase earlier than 90 A. Although the network hindrance caused SBS MA had a higher concentration of aging functional groups than 90 A at some times, like 12 h and 48 h, the total increase and decrease of aging functional groups were significantly lower than 90 A. This manifested that SBS MA had better oxidation, dissolution and migration resistance.

Based on the change of $I_{C=O}$ at different depths, the erosion depth by moisture could be observed as shown in Fig. 5. After immersion for 4, 6, 12, 48, 96, 144, 288, 366, 432 and 504 h, the erosion depth of 90 A reached 27, 49, 108, 161, 214, 168, 294, 385, 432 and 519 μm, respectively. Simultaneously, the erosion depth of SBS MA reached 23, 47, 70, 130, 205, 253, 234, 308, 353 and 374 μm. The relation between

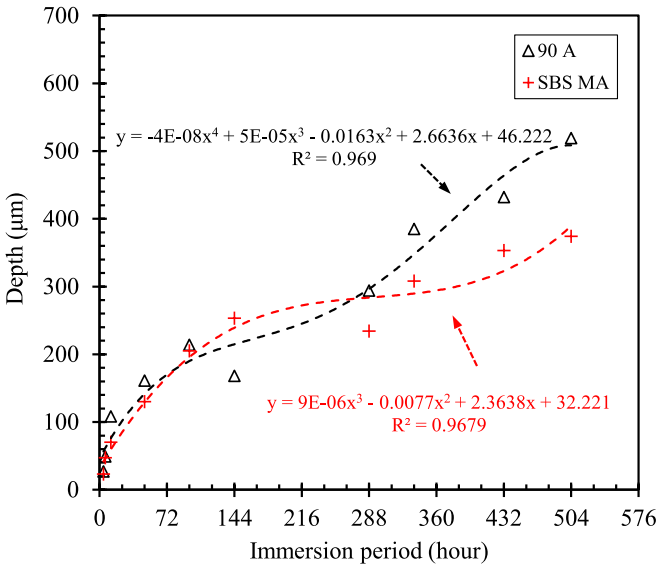

Fig. 5. Relation between erosion depth and immersion period (for $I_{C=O}$).

erosion depth and immersion period was suitable for a polynomial model to regression fitting, and the R^2 was bigger than 0.9. The erosion depth increased over immersion period, and it was evident that moisture intrusion was a gradual infiltration process. And the erosion depth growth was first urgent, then slow and finally urgent, indicating that erosion may be a cyclical process. The erosion depth of SBS MA was less than that of 90 A. According to diffusion theory, when there is a concentration gradient within a substance, the internal particles of the substance will undergo a directional migration due to thermal motion, and the larger the gradient, the larger the diffusion rate [41]. Combined with Fig. 4, it could be seen that the larger change rate in $I_{C=O}$ made 90 A had a larger difference between the eroded layer and the internal uneroded layer, resulting in a larger erosion depth.

3.2. Rheological property

Moisture erosion can change the rheological property, and the changes have fluctuation due to the combination of asphalt oxidation, dissolution and migration [26]. Fatigue performance changes are an important indicator of the degree of asphalt aging [33,42]. The G*sinδ at 28 °C was taken for the *FF* to conclude the fatigue resistance change of asphalt binders at different depths. After immersion for different periods, the *FF* of 90 A and SBS MA at different depths were calculated as shown in Fig. 6. The *FF* of the unsoaked control group slightly increased with preparation time, because the asphalt oxidation increased the $I_{C=O}$ hardening the asphalt. The *FF* of all layers in 90A was greater than the control value during the 4–96 h of immersion, indicating that the oxidative aging of asphalt caused by water erosion increased the *FF* of asphalt. The *FF* in each layer of 90 A increased in a step-like manner with the extension of erosion period, however the increasing rate decreased step by step from the surface to the inside. After immersion for 4, 6 and 96 h, the *FF* of the layer 1 was the largest, and the layer 2 had the biggest *FF* after 12 and 48 h. Compared with the control at 144 h, the *FF* of layers 1–3 decreased, while that of layers 4–6 increased, which might be the increase of *FF* caused by aging spread to layers 4–6, and the dissolution of polar components decreased the *FF* of layers 1–3. During 288 h-504 h of immersion, due to the dominance of dissolution and migration, the *FF* decreased, and the decline decreased step by step from surface to inside.

The *FF* of SBS MA was greater than the control during 4–48 h, and the *FF* of each layer increases in a step-like manner with the extension of erosion period. After immersion for 4, 6 and 48 h, the layer 1 had the biggest *FF*, and the layer 2 at 12 h of immersion had the biggest *FF*.

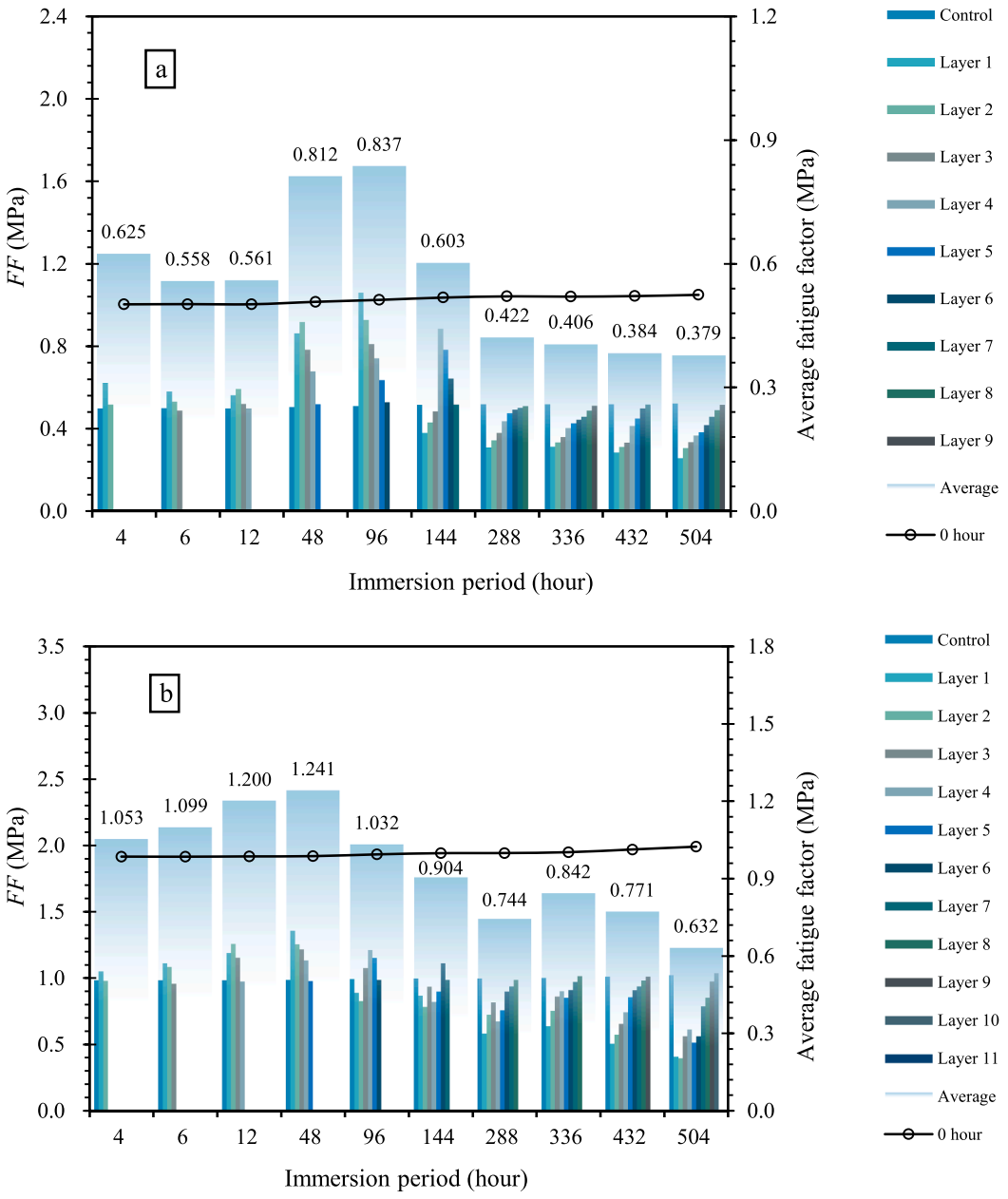

Fig. 6. *FF* of asphalt at different depths during immersion (a, 90 A; b, SBS MA).

Compared with the control at 96 h, the *FF* of layers 1–2 decreased, while that of layers 3–5 increased, which might be probably for the $I_{C=O}$ change at 96 h. At 144 h, the *FF* of layers 3–5 began to decrease, and the *FF* of layer 6 increased compared with the control, while the average value became to be less than the control value. The *FF* of layers 1–7 at 288 h and 336 h of immersion fluctuated up and down, and the *FF* of layers 2 and 3 at 288 h were bigger than that of adjacent layers, so were that of layers 3 and 4 at 336 h. During 96–336 h of immersion, the *FF* changes showed that the existence of network structure caused the rheological property of SBS MA more complex than that of 90A. During 432 h of immersion, the *FF* decreased due to the dominance of dissolution, and the decline decreased in a step-like manner from surface to inward. After immersion for 504 h, the *FF* of all layers declined to lower than that of control, and layers 3 and 4 had the *FF* larger than the surrounding layers.

The average *FF* of 90 A peaked at 96 h of immersion increasing by 63.32 %, and reached a trough decreasing by 27.75 % after 432 h of immersion. The average *FF* of SBS MA at 48 h increased to the maximum value by 28.71 %, and it decreased to the minimum value by 39.00 % at 432 h. The maximum increment of SBS MA was less than that of 90A, but the maximum decrement was greater than SMS MA. This might be explained by the fact that the C=C of SBS broke in SBS MA after immersion.

Based on the *FF*, the relation between erosion depth and immersion period could be described as shown in Fig. 7. After immersion for 4, 6, 12, 48, 96, 144, 288, 366, 432 and 504 h, the erosion depth of 90 A reached 27, 49, 108, 161, 214, 281, 352, 385, 277 and 391 μm, while the erosion depth of SBS MA reached 23, 47, 70, 130, 205, 253, 293, 308, 322 and 353 μm, respectively. The relation between erosion depth and period was suitable for the cubic equation to regression fitting, and the R^2 was bigger than 0.9. The growth rate in 90 A and SBS MA declined with period, and the growth rate and erosion depth in SBS MA was less than that in 90 A. Compared with the FTIR analysis, the turning point of the *FF* change was earlier than the $I_{C=O}$. It might be because of the moisture erosion could also change the overall microstructure of asphalt, and the rheological properties of asphalt were affected by the

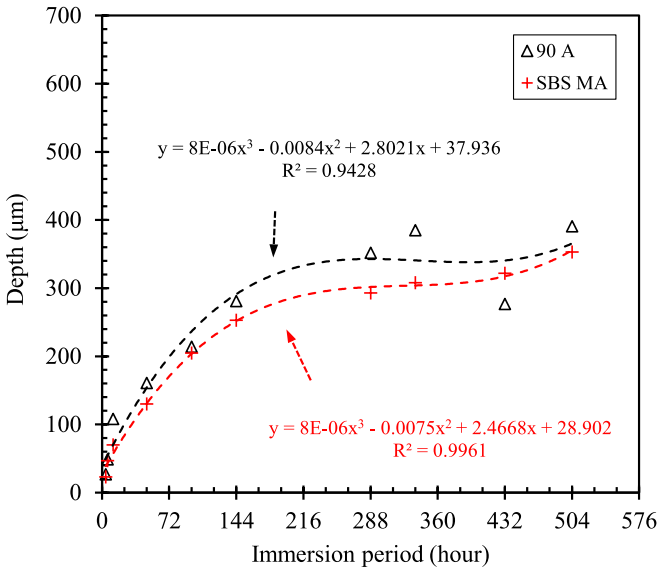

Fig. 7. Relation between erosion depth and immersion period (for *FF*).

microscopic structure in addition to C═O.

3.3. Adhesion property

The CA is directly related to the surface wettability, and the diagram of CA measurement was presented in Fig. 8. The internal angle between the probe liquid and the sample to be measured is defined as the CA. The 90° (θ = 90°) is the boundary of wettability. When the CA is higher than 90° (θ > 90°), it indicates that the probe liquids have poor wettability. If the CA is less than 90° (θ < 90°), it manifests that the solvent is wetting the surface. The results of CA test of the layer 1 immersed for different periods were present in Table. 6. As could be seen from the table, the θ between control with distilled water was greater than 90°, and θ had no evident changes with preparation time. It indicated that 90 A and SBS MA belonged to hydrophobic material. After immersion, the CAs showed a downward trend. According to surface energy theory, the CA between asphalt and water can represent the wettability of asphalt and then reflect the water-damage resistance property of asphalt [43]. It indicated that the wettability of asphalt to distilled water increased over immersion period, which was detrimental to the water damage resistance of asphalt. The CA of 90 A immersed for 432 h decreased by 5. 26 % to reach the lowest value, while that of SBS MA immersed for 504 h decreased by 3.78 %.

In asphalt mixtures, the asphalt-aggregate adhesion affects the moisture damage resistance of the asphalt-aggregate interface. Herein, the *ER* of different layers were be calculated by the contact angle as illustrated in Fig. 9. The *ER* is the ratio of the W_{am} and W_{amw} and is used to evaluate the adhesion property of asphalt. The higher the *ER* value, the better the adhesion property of the asphalt-aggregate combination. The *ER* of all layers in 90A was greater than control during 0–288 h, the

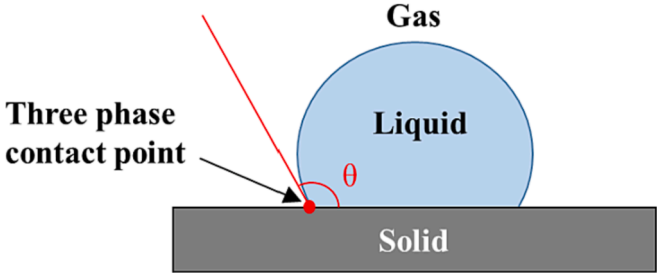

Fig. 8. Diagram of CA measurement.

Table 6
CAs of 90 A and SBS MA after immersion (°).

Period (h)	90 A		SBS MA	
	Control	Distilled water	Control	Distilled water
4	93.5	92.9	92.1	91.8
6	93.0	92.6	92.5	91.6
12	93.5	92.6	92.8	91.9
48	93.0	91.6	92.0	91.5
96	93.4	91.1	92.4	90.8
144	93.3	91.9	92.7	90.1
288	93.1	91.6	92.3	90.2
336	93.2	91.5	92.7	90.0
432	93.1	88.2	92.9	89.4
504	93.2	91.8	92.6	89.1

Note: The CV of all CAs in parallel tests was lower than 4.00%.

ER in each layer of asphalt was close to the control step by step with depth. This phenomenon may be due to the increase of polar components caused by oxidative aging during moisture erosion, which increases the adhesion of asphalt [44]. Among them, the layer 2 at 96 h was the largest, and the rest of the layer 1 was the largest. The *ER* of each layer immersed for 336 h was greater than the control, but layer 3 was smaller than the surrounding layer. After immersion for 432 h, the *ER* of all layers except layer 5 was greater than control. The *ER* of each layer immersed for 504 h was smaller than the control, but the layer 4 was larger than the surrounding layer. It illustrated that the phenomenon of asphalt film stripping was likely to occur at these depths.

During 0–48 h of immersion, the *ER* of all layers in SBS MA were greater than control. The *ER* at 96 h was slightly reduced, the layers 1–3 were roughly the same size, and the layers 4 and 5 were greater than the control sample. Each layer immersed for 144–432 h decreased, and each layer stepped towards control with depth. At 504 h of immersion, each layer was smaller than the control sample, however the layer 4 was greater than the surrounding layer. It illustrated that the phenomenon of asphalt film stripping was likely to occur at these depths.

The variation pattern of the average *ER* was correlated with that of the first layer. The average *ER* of 90 A peaked at 144 h of immersion increasing by 10.72 %, and reached a trough decreasing by 2.79 % after 504 h of immersion. The average *ER* of SBS MA at 12 h increased to the maximum value by 1.51 %, and it decreased to the minimum value by 8.37 % at 144 h. The minimum *ER* of SBS MA was still greater than 90A, however the decrease of SBS was greater than 90, indicating that the adhesion property of SBS MA was more easily affected by moisture.

Based on the data, the change rule of erosion depth with immersion period was displayed in Fig. 10. The relation between erosion depth and period was suitable for polynomial model to regression fitting, and the R^2 was bigger than 0.9. After immersion for 4, 6, 12, 48, 96, 144, 288, 366, 432 and 504 h, the erosion depth of 90 A reached 27, 23, 60, 161, 167, 281, 294, 385, 432 μm and 391 μm, while that of SBS MA reached 23, 47, 70, 130, 205, 253, 234, 308, 322 and 374 μm, respectively. The erosion depth of SBS MA was less than that of 90 A, which consisted with the result of FTIR test and DSR test. The possibility that the unstable behavior of every layer might be caused by experimental errors could not be denied. Therefore, three characteristics were used to verify each other. Only in this case can a convincing conclusion be drawn. Compared with the FTIR and DSR analysis, the *ER* of 90 A began to decline after immersion for 504 h, which was later than the $I_{C=O}$ and *FF*. The phenomenon might be explained by the fact that moisture erosion could also change the microstructure of asphalt, and the adhesion property were affected by rheological properties and the chemical structure. Thereby, there was a lag in the macro between the change law of adhesion property with rheological properties and chemical structure.

3.4. Correlation analysis between $I_{C=O}$, FF and ER

Table 7 illustrated the correlation analysis results between $I_{C=O}$, *FF*

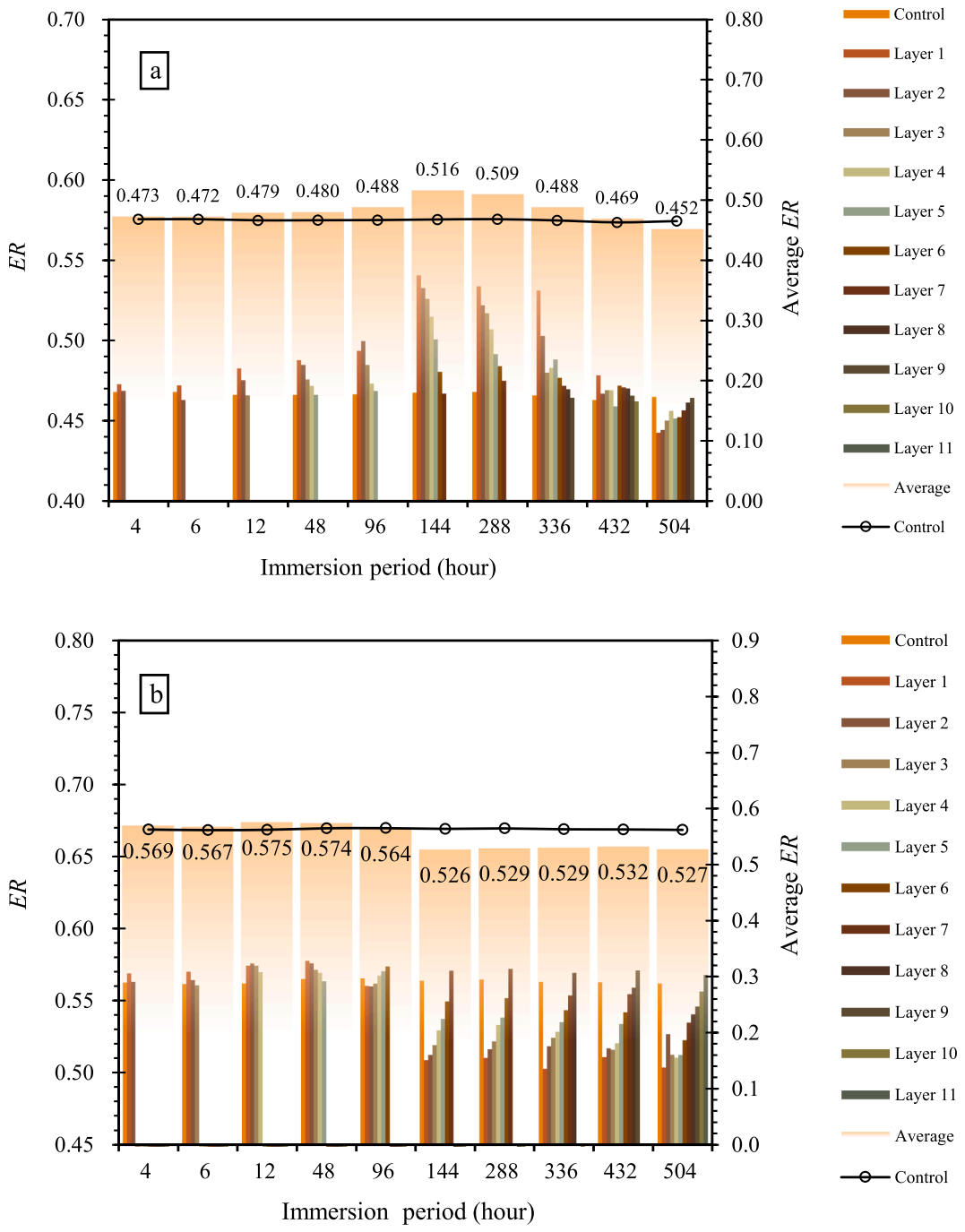

Fig. 9. *ER* of asphalt at different depths during immersion (a, 90 A; b, SBS MA).

and *ER* obtained by processing with software SPSS 22.0. The parameter r represented Pearson correlation coefficient between two variates, and the parameter p represented significance of correlation between two variates. And when $p < 0.01$, the correlation was significant. Therefore, the correlation between $I_{C=O}$ and *FF* of 90 A was significant, while that between the $I_{C=O}$ and *FF*, $I_{C=O}$ and *ER* and *FF* and *ER* of SBS MA were significant. And the order of parameter r was as follow, *FF-ER* of SBS MA (0.837) > $I_{C=O}$-*FF* of 90 A (0.756) > $I_{C=O}$-*FF* of SBS MA (0.675) > $I_{C=O}$-*ER* of SBS MA (0.591). It could be judged that all four relations were positively correlation, and the correlation between *FF* and *ER* of SBS MA was maximized, while that between $I_{C=O}$ and *ER* of SBS MA was minimized. Subsequently, the regression analysis was conducted on the four kinds of relation as illustrated in Fig. 11. The R^2 were all less than 0.9 due to the discreteness of data. Significantly, the correlation between $I_{C=O}$ and *FF* of 90A was clear when the $I_{C=O}$ was less than 0.7 %. And the correlation between $I_{C=O}$ and *FF* of SBS MA and $I_{C=O}$ and *ER* of SBS MA was obvious when the $I_{C=O}$ was greater than 0.8 %. The data of *FF* and *ER* in SBS MA were evenly distributed and the fitting equation could be used as a reference. It indicated that the $I_{C=O}$ of 90 A could be applied to predict the *FF* when $0 < I_{C=O} < 0.7$ %. And the $I_{C=O}$ of SBS MA could be employed in predicting the *FF* and *ER* when 0.8 % < $I_{C=O}$ < 1.4 %, and *FF* and *ER* could be predicted each other.

3.5. Diffusion coefficient of eroded asphalt

By exploring the diffusion coefficient of eroded asphalt during moisture erosion, the diffusion dynamic process of asphalt erosion can be characterized to a certain extent, and the mechanism of erosion

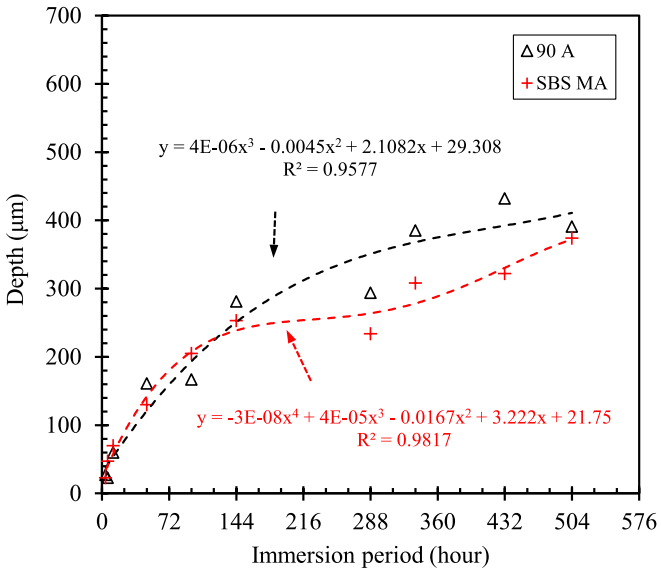

Fig. 10. Relation between erosion depth and immersion period (for *ER*).

Table 7
Correlation coefficient between $I_{C=O}$, *FF* and *ER* of 90A and SBS MA (n = 76).

		$I_{C=O}$		*FF*		*ER*	
		r	p	r	p	r	p
90 A	$I_{C=O}$	1.000	NA	0.756**	0.000	0.220	0.056
	FF	0.756**	0.000	1.000	NA	0.084	0.470
	ER	0.220	0.056	0.084	0.470	1.000	NA
SBS MA	$I_{C=O}$	1.000	NA	0.675**	0.000	0.591**	0.000
	FF	0.675**	0.000	1.000	NA	0.837**	0.000
	ER	0.591**	0.000	0.837**	0.000	1.000	NA

Note: ** Correlation is significant p at the 0.01 level (2-tailed).

Correlation is significant p at the 0.01 level (2-tailed).

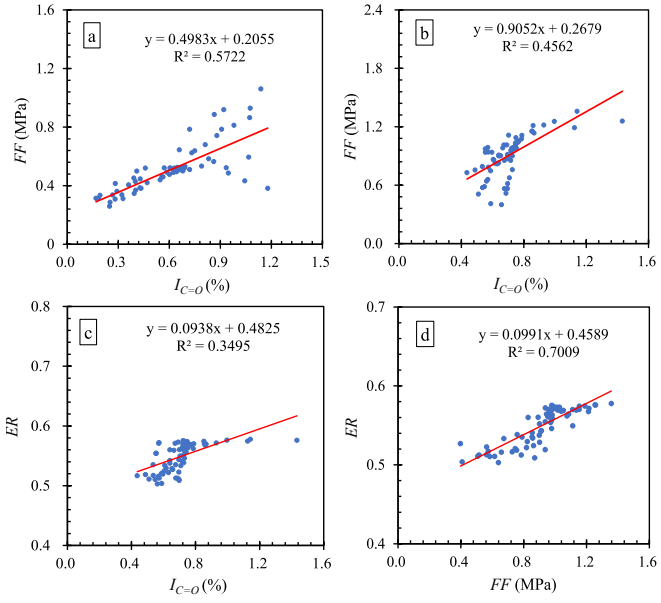

Fig. 11. Correlation between $I_{C=O}$, *FF* and *ER* of 90 A (a) and SBS MA (b, c and d).

asphalt changing with immersion period can be discussed, which has important theoretical and practical significance for the parameter selection of laboratory immersion test. It is found that when the $I_{C=O}$ is less than or equal to 0.01, and the order of magnitude variation of *ER* is small, it is considered that the error is too large to calculate *D* [40]. Therefore, *FF* is more suitable for calculating the *D* of eroded asphalt, which was calculated by substituting the *FF* into the Eq. (10)–(12). The |FF| of control sample, the first layer and other layers was considered to be the $|FF|_U$, $|FF|_E$ and $|FF|_D$, respectively. Table 8 illustrated the *D* of 90 A at different depths during immersion, and the magnitude order of *D* was 10^{-4}–10^{-1} μm²/s. It was known from Fig. 6. a, that there was a phenomenon that the *FF* of some layers was above, while that of else layers was below that of control at 144 h of immersion. It was inconvenient to calculate *D* and therefore not discussed. The maximum *D* at each period was marked in bold, and it is found that the depth where the maximum *D* was located increased with period from 0 to 336 h, indicating that moisture erosion slowly spread to the deeper asphalt during this erosion stage. And the maximum *D* at 432 and 504 h was again in layers 3 and 4, indicating that probably 0–336 h was the first erosion cycle, while 432 starts the next cycle, indicating that the moisture erosion process on asphalt was cyclical.

Table 9 illustrated the *D* of SBS MA at different depths during immersion, and the order of magnitude of *D* was 10^{-4}–10^{-1} μm²/s. It was known from Fig. 6b, that there was a phenomenon that the *FF* of some layers was above, while that of else layers was below that of control at 96 h of immersion. And the *FF* of all layers except layer 6 was bigger than that of control at 144 h of immersion. It was inconvenient to calculate *D* and therefore the *D* of all layers at 96 h and layer 6 at 144 h were not discussed. During 0–144 h, the depth where the maximum *D* was located increased with period, indicating that moisture erosion slowly spread to the deeper asphalt during this phase. The maximum *D* at 288–432 h was again in layers 4, 5 and 7, and that at 504 h was layer 5, indicating that probably 0–144 h was the first erosion cycle, while 288–432 h was the second cycle and 504 starts the next erosion cycle again. Combined with the analysis in FTIR, DSR and CA tests, it was possible that the mesh structure of SBS reduce the migration rate of polar components from the surface asphalt to the inner asphalt, and blocked the dissolution and migration of asphalt components, resulting in a shorter erosion cycle period.

The oxidation reaction of asphalt with oxygen molecules in water can produce the polar molecules [20,29]. Due to the polarity of water, the polar components in asphalt are more likely to be dissolved and migrated, resulting in a gradual reduction of polar components during immersion [30]. A combination of FTIR, DSR and CA tests revealed that asphalt oxidation was dominant in the early stage of immersion, probably due to the fewer polar components in asphalt at this time. At the later stage, the polar components generated by asphalt oxidation accumulation gradually increased to a certain extent, so much that the dissolution and migration of asphalt began to dominate. The asphalt component ratio was constantly changing, because the oxidation, dissolution and migration of asphalt occurred alternately in asphalt. That might be the reason why the erosion behavior of the asphalt by water showed cyclical.

4. Conclusions

In this study, the effect of moisture and immersion period on asphalt binder of different depths was investigated to the moisture erosion depth on asphalt and the relate mechanism analysis. And FTIR, DSR and CA tests were conducted to monitor the changes in chemical component, rheological properties and adhesion property respectively. The following conclusions can be drawn:

(1) The entire asphalt film with the thickness of pavement in reality have been eroded by moisture after 4 h of immersion. As the erosion period increased, the performance changes present a

Table 8
D of 90 A at different depths during immersion (10^{-1} μm^2/s).

Layer	Immersion period (hour)							
	6	12	48	96	288	336	432	504
2	**0.101**	0.080	0.206	0.052	0.015	0.028	0.019	0.007
3	NA	**0.461**	**1.583**	0.196	0.067	0.103	**0.089**	0.044
4	NA	NA	0.992	**0.409**	0.076	0.114	0.049	0.087
5	NA	NA	NA	0.352	0.086	0.163	0.066	**0.141**
6	NA	NA	NA	NA	0.102	0.203	0.051	0.139
7	NA	NA	NA	NA	**0.127**	**0.237**	NA	0.123
8	NA	NA	NA	NA	NA	0.186	NA	0.108

Table 9
D of SBS MA at different depths during immersion (10^{-1}μm^2/s).

Layer	Immersion period (hour)							
	6	12	48	144	288	336	432	504
2	**1.429**	0.144	0.057	0.001	0.004	0.004	0.011	0.387
3	NA	**5.516**	0.337	0.036	0.013	0.011	0.025	0.030
4	NA	NA	**0.426**	0.274	**0.363**	0.033	0.049	0.073
5	NA	NA	NA	**2.016**	0.236	**0.133**	0.055	**0.573**
6	NA	NA	NA	NA	0.099	0.126	0.068	0.483
7	NA	NA	NA	NA	0.109	0.106	**0.089**	0.142
8	NA	NA	NA	NA	NA	NA	0.079	0.135
9	NA	NA	NA	NA	NA	NA	NA	0.076

stepwise trend from surface to interior. And the relation between erosion depth and immersion period is suitable for polynomial model to regression fitting. It can be divided into three stages, the growth process of erosion depth that is first urgent and then slow and finally urgent. The depth growth of 90 A is greater than that of SBS MA.

(2) During 0–504 h of immersion period, oxidation, dissolution and migration of asphalt occur alternately, resulting in a fluctuation reduce of the $I_{C=O}$, *FF* and *ER* of asphalt after TFOT Oxidation, dissolution and migration of asphalt occur alternately leading to a fluctuation of the $I_{C=O}$, *FF* and *ER* from large to small during 0–504 h of immersion period. At the macroscopic level, there is a lag between the changes in adhesion property and the other two properties. According to the correlation analysis, the correlation between $I_{C=O}$ and *FF* of 90A is clear when the $I_{C=O}$ is less than 0.7 %. And the correlation between $I_{C=O}$ and *FF* of SBS MA and $I_{C=O}$ and *ER* of SBS MA is obvious when the $I_{C=O}$ is greater than 0.8 %. During the whole immersion cycle, the correlation between FF and ER of SBS MA is satisfied, and the fitting equation can be used as a reference.

(3) According to the calculation of diffusion coefficient, the moisture erosion process on asphalt is found to be cyclical. During immersion, the magnitude order of *D* in 90 A and SBS MA are 10^{-4}–10^{-1}μm^2/s. The mesh structure of SBS reduces the migration rate of polar components from the surface asphalt to the inner asphalt, and blocks the dissolution and migration of asphalt components, resulting in a shorter erosion cycle period.

The diffusion mechanism can provide a theoretical basis for the development of laboratory moisture erosion test specification and anti-moisture damage technology. However, oxidation, dissolution and migration of asphalt may occur simultaneously at different depths during moisture erosion, so that the Loglog model was not suitable for simulation of the phenomenon. Therefore, future research can start with a model more suitable for simulating this phenomenon.

CRediT authorship contribution statement

Yingxue Zou: Conceptualization, Writing – original draft. **Haiqin Xu:** Data curation, Software. **Shi Xu:** Methodology. **Anqi Chen:** Writing – review & editing. **Shaopeng Wu:** Investigation. **Serji Amirkhanian:** Investigation, Data curation. **Pei Wan:** Methodology. **Xiang Gao:** .

Declaration of Competing Interest

The authors declare that they have no known competing financial interests or personal relationships that could have appeared to influence the work reported in this paper.

Data availability

The data that has been used is confidential.

Acknowledgements

This work was supported by the National Key R&D Program of China [No. 2018YFB1600200]; the Technological Innovation Major Project of Hubei Province [2019AEE023]; the Independent Innovation Foundation of Wuhan University of Technology [223131001]; and the Key R&D Program of Hubei Province [2020BCB064].

References

[1] N. Li, Q. Jiang, F. Wang, P. Cui, J. Xie, J. Li, S. Wu, D. Barbieri, Comparative assessment of asphalt volatile organic compounds emission from field to laboratory, J. Cleaner Prod. 278 (2021).
[2] Y. Lv, S. Wu, P. Cui, Q. Liu, Y. Li, H. Xu, Y. Zhao, Environmental and feasible analysis of recycling steel slag as aggregate treated by silicone resin, Constr. Build. Mater. 299 (2021).
[3] A.R. Pasandin, I. Perez, A. Ramirez, M.M. Cano, Moisture damage resistance of hot-mix asphalt made with paper industry wastes as filler, J. Cleaner Prod. 112 (2016) 853–862.
[4] L. Li, Z. Zhang, Z. Wang, Y. Wu, Y. Zhang, Coupled thermo-hydro-mechanical response of saturated asphalt pavement, Constr. Build. Mater. 283 (2) (2021), 122771.
[5] J. Cai, Y. Wen, D. Wang, R. Li, J. Xie, Investigation on the cohesion and adhesion behavior of high-viscosity asphalt binders by bonding tensile testing apparatus, Constr. Build. Mater. 261 (2020).
[6] P. Chaturabong, H.U. Bahia, Effect of moisture on the cohesion of asphalt mastics and bonding with surface of aggregates, Road Mater. Pavement Des. 19 (3–4) (2018) 741–753.
[7] Y. Zou, S. Amirkhanian, S. Xu, Y. Li, Y. Wang, J. Zhang, Effect of different aqueous solutions on physicochemical properties of asphalt binder, Constr. Build. Mater. 286 (2021).

[8] P. Wan, Q. Liu, S. Wu, Z. Zhao, X. Yu, A novel microwave induced oil release pattern of calcium alginate/ nano-Fe3O4 composite capsules for asphalt self-healing, J. Cleaner Prod. 297 (2) (2021), 126721.
[9] F. Wang, J. Xie, S. Wu, J. Li, D.M. Barbieri, L. Zhang, Life cycle energy consumption by roads and associated interpretative analysis of sustainable policies, Renew. Sust. Energ. Rev. 141 (2021).
[10] B. Sengoz, E. Agar, Effect of asphalt film thickness on the moisture sensitivity characteristics of hot-mix asphalt, Build. Environ. 42 (10) (2007) 3621–3628.
[11] H. Zhang, J.T. Harvey, L. Jiao, H. Li, M. Elkashef, Study on binder film thickness distribution of recycled asphalt pavements, J. Test. Eval. (2019).
[12] L. Rezende, S.R. Kommidi, Y.R. Kim, M. Khedmati, Strain sweep fatigue testing of sand asphalt mortar to investigate the effects of sample geometry, binder film thickness, and testing temperature, Transportt. Res. Rec. (2021) 036119812110116.
[13] C. Yang, S. Wu, P. Cui, S. Amirkhanian, Z. Zhao, F. Wang, L. Zhang, M. Wei, X. Zhou, J. Xie, Performance characterization and enhancement mechanism of recycled asphalt mixtures involving high RAP content and steel slag, J. Cleaner Prod. 336 (2022).
[14] J. Li, J. Yu, S. Wu, J. Xie, The mechanical resistance of asphalt mixture with steel slag to deformation and skid degradation based on laboratory accelerated heavy loading test, Materials (Basel) 15 (3) (2022).
[15] F. Li, Y. Yang, L. Wang, Evaluation of physicochemical interaction between asphalt binder and mineral filler through interfacial adsorbed film thickness, Constr. Build. Mater. 252 (8) (2020), 119135.
[16] H. Xu, Y. Zou, S. Wu, H. Li, S. Xu, Y. Zhao, Y. Lv, Research on gradient characteristics and its prediction method of induction heating asphalt concrete, Constr. Build. Mater. 309 (2021).
[17] S. Dos Santos, M.N. Partl, L.D. Poulikakos, Newly observed effects of water on the microstructures of bitumen surface, Constr. Build. Mater. 71 (2014) 618–627.
[18] C. Yan, W. Huang, Q. Lv, Study on bond properties between RAP aggregates and virgin asphalt using Binder Bond Strength test and Fourier Transform Infrared spectroscopy, Constr. Build. Mater. 124 (2016) 1–10.
[19] N. Lin, Influence of asphalt film thickness on pavement performance of drainage pavement, Sichuan Build. Mater. 38 (6) (2012) 170–172.
[20] L. Pang, X. Zhang, S. Wu, Y. Ye, Y. Li, Influence of water solute exposure on the chemical evolution and rheological properties of asphalt, Materials (Basel) 11 (6) (2018).
[21] P. Cui, S. Wu, Y. Xiao, R. Hu, T. Yang, Environmental performance and functional analysis of chip seals with recycled basic oxygen furnace slag as aggregate, J. Hazard. Mater. 405 (2021), 124441.
[22] D. Astm, Standard test method for penetration of bituminous materials, ASTM International, USA, 2013.
[23] A. Standard, D36, Standard test method for softening point of bitumen (ring-and-ball apparatus), ASTM International, West Conshohocken, USA (2009).
[24] ASTM, Standard test method for ductility of bituminous materials, (2007).
[25] ASTM, Standard test method for solubility of asphalt materials in trichloroethylene, ASTM International West Conshohocken, PA2015.
[26] H. Yang, L. Pang, Y. Zou, Q. Liu, J. Xie, The effect of water solution erosion on rheological, cohesion and adhesion properties of asphalt, Constr. Build. Mater. 246 (2020).
[27] AASHTO, Standard method of test for determining the rheological properties of asphalt binder using a dynamic shear rheometer (DSR), T 315. AASHTO, Washington DC. (2019).
[28] L.R. Luo J, Tu C, Effect of relative humidity on the adhesion between asphalt and aggregate, J. Wuhan Univ. Tech. 45(4) (2021).
[29] J.A. Hernández Noguera, H.A. Rondón Quintana, W.D. Fernández Gómez, The influence of water on the oxidation of asphalt cements, Constr. Build. Mater. 71 (2014) 451–455.
[30] I. Menapace, E. Masad, The influence of moisture on the evolution of the microstructure of asphalt binders with aging, Road Mater. Pavement Des. 21 (2) (2018) 331–346.
[31] A. Chen, Z. Hu, M. Li, T. Bai, G. Xie, Y. Zhang, Y. Li, C. Li, Investigation on the mechanism and performance of asphalt and its mixture regenerated by waste engine oil, Constr. Build. Mater. 313 (2021).
[32] Z. Zhao, S. Wu, Q. Liu, J. Xie, C. Yang, F. Wang, P. Wan, Recycling waste disposable medical masks in improving the performance of asphalt and asphalt mixtures, Constr. Build. Mater. 337 (2022).
[33] Y. Zhao, M. Chen, S. Wu, Q. Jiang, H. Xu, Z. Zhao, Y. Lv, Effects of waterborne polyurethane on storage stability, rheological properties, and VOCs emission of crumb rubber modified asphalt, J. Cleaner Prod. 340 (2022).
[34] S. Liu, S. Zhou, A. Peng, Analysis of moisture susceptibility of foamed warm mix asphalt based on cohesion, adhesion, bond strength, and morphology, J. Cleaner Prod. 123334 (2020).
[35] D.K. Owens, R.C. Wendt, Estimation of the surface free energy of polymers, J. Appl. Polym. Sci. 13 (8) (1969).
[36] L. Wang, Y. Jia, D. Zhang, J. Hu, Influence of salt freezing cycle on interfacial adhesion of asphalt-aggregate based on surface energy theory, Acta Mater. Compos. Sin. (2016).
[37] Y. Tan, M. Guo, Using surface free energy method to study the cohesion and adhesion of asphalt mastic, Constr. Build. Mater. 47 (2013) 254–260.
[38] M. Izadmehr, M. Abbasi, M. Mansouri, A. Kazemi, A. Nakhaee, A. Daryasafar, Accurate analytical model for determination of effective diffusion coefficient of polymer electrolyte fuel cells by designing compact Loschmidt cells, Fuel 199 (2017) 551–561.
[39] H. Lehtimäki, Rejuvenating RAP with light oil products and a new mixing method for hot in-plant recycling, 21st Nordic Road Congress, Reykjavík, Iceland, 2012.
[40] W. Zeng, Research on Mechanism and Characterization for Ultraviolet Aging of Asphalt, Wuhan University of Technology, China, 2017.
[41] A.G. Kesarev, V.V. Kondratyev, I.L. Lomaev, The theory of diffusion zone formation during surface modification of materials with allowance for the thermodiffusion effects, Phys. Met. Metall. 122 (2) (2021) 134–140.
[42] Y. Li, J. Feng, F. Yang, S. Wu, Q. Liu, T. bai, Z. Liu, C. Li, D. Gu, A. Chen, Y. Jin, Gradient aging behaviors of asphalt aged by ultraviolet lights with various intensities, Constr. Build. Mater. 295 (2021).
[43] P. Caputo, D. Miriello, A. Bloise, N. Baldino, O. Mileti, G.A. Ranieri, A comparison and correlation between bitumen adhesion evaluation test methods, boiling and contact angle tests, Int. J. Adhes. Adhes. 102 (2020).
[44] P. Mikhailenko, C. Kou, H. Baaj, L. Poulikakos, A. Cannone-Falchetto, J. Besamusca, B. Hofko, Comparison of ESEM and physical properties of virgin and laboratory aged asphalt binders, Fuel 235 (2019) 627–638.